Surface Assisted Combustion of Hydrogen-Oxygen Mixture in Nanobubbles Produced by Electrolysis

Alexander Prokaznikov [1,2], Niels Tas [3] and Vitaly Svetovoy [1,4,*]

1   Yaroslavl Branch of the Institute of Physics and Technology, Russian Academy of Sciencies,
    150007 Yaroslavl, Russia; prokaznikov@mail.ru
2   P. G. Demidov Yaroslavl State University, Sovetskaya 14, 150000 Yaroslavl, Russia
3   MESA$^+$ Institute for Nanotechnology, University of Twente, PO Box 217, 7500 AE Enschede,
    The Netherlands; n.r.tas@utwente.nl
4   Zernike Institute for Advanced Materials, University of Groningen, Nijenborgh 4,
    9747 AG Groningen, The Netherlands
*   Correspondence: v.b.svetovoy@rug.nl; Tel.: +31-50-363-4972

Abstract: The spontaneous combustion of hydrogen–oxygen mixture observed in nanobubbles at room temperature is a puzzling phenomenon that has no explanation in the standard combustion theory. We suggest that the hydrogen atoms needed to ignite the reaction could be generated on charged sites at the gas–liquid interface. Equations of chemical kinetics augmented by the surface dissociation of hydrogen molecules are solved, keeping the dissociation probability as a parameter. It is predicted that in contrast with the standard combustion, the surface-assisted process can proceed at room temperature, resulting not only in water, but also in a perceptible amount of hydrogen peroxide in the final state. The combustion time for the nanobubbles with a size of about 100 nm is in the range of 1–100 ns, depending on the dissociation probability.

Keywords: nanobubbles; combustion; dissociation

PACS: 47.55.D-; 82.33.Vx; 82.65.+r; 85.85.+j

1. Introduction

Combustion processes are supported by the heat produced by the combustion reactions [1–4]. For a small volume of the reaction chamber, the surface-to-volume ratio becomes large, and the heat escapes from the volume too quickly to sustain the combustion. Quenching of the reactions is the main obstacle for scaling down internal combustion engines [5,6], which could be used to power different kinds of micro and minidevices [7,8]. Nevertheless, combustion of a stoichiometric mixture of hydrogen and oxygen was recently observed in nanobubbles [9,10] and at special conditions in microbubbles [11,12]. The reaction between gases is ignited spontaneously at room temperature, and cannot be explained by the standard combustion process. The high density of nanobubbles observed in the experiments suggests that the reaction is a surface-assisted process [13], but no specific mechanism has ever been discussed.

Here we propose a mechanism for the combustion of the hydrogen–oxygen mixture in nanobubbles. The mechanism is related to charges existing on the gas–electrolyte interface. These charges provide sites where H_2 (and possibly O_2) molecules dissociate, producing H and O atoms in the gas phase. These atoms ignite and support the combustion reactions. The main prediction of the model that can be directly checked experimentally is that the surface-assisted combustion produces an appreciable amount of hydrogen peroxide, in contrast with the normal combustion.

Nanobubbles containing a mixture of gases were produced by the alternating polarity electrolysis when the voltage polarity of an electrode changes with a frequency $f \sim 100$ kHz. In this case, a thin layer adjacent to the electrode is highly supersaturated with both gases [9]. Nanobubbles that are formed in the layer do not grow large, and disappear in phase with the electrical pulses. Periodic reduction of the gas concentration was observed in different systems with a vibrometer [9,10]. Direct observation of the nanobubbles was not possible due to the small size (~ 100 nm) and short lifetime (~ 1 μs) of the objects. However, at some conditions [11,12] the nanobubbles can merge to form a visible short-lived microbubble, which is also ignited spontaneously and disappears with a significant release of energy.

Energy production on the time scale of microseconds provides proof that the observed process is the combustion but not just conversion of the gases. The reaction between H_2 and O_2 gases in nanobubbles produces heat that cannot be explained by the Joule heating of the electrolyte. Because the heat escapes very quickly to the liquid and solid substrates, the temperature rise around the electrodes was expected less than $1\ ^\circ$C. Nevertheless, it was measured by a gold probe located in the vicinity of the electrodes [9]. In an independent study [14], the effect was investigated in detail using a built-in thermal microsensor. Much stronger heating—up to $50\ ^\circ$C—was observed in a microchamber covered with a flexible membrane [10]. A significant heating due to a small thermal mass of the device was measured using the thermal dependence of the current passing through the electrolyte.

At high nanobubble density, they start to coalesce and form short-lived microbubbles. In a closed microchamber, the bubbles with a size of 5–10 μm last for just a few microseconds [11]. Each microbubble is accompanied by a pressure jump in the chamber, so the combustion energy was transformed not only to the heat, but also to the enthalpy of the liquid and to the mechanical work done by the flexible membrane. For an open millimeter-scale system, the microbubbles formed by coalescence have original size of 40 μm, combustion happens in less than 10 μs, and produces a well-audible sound (click) [12]. The bubble inflates during 50 μs to a size of 300 μm, and the main part of the combustion energy is transformed to mechanical work done by the inflating bubble. The mechanism of combustion in microbubbles is related in some way to their origin from merging nanobubbles: the reaction is not ignited in bubbles with a size of 10 μm produced by a microfluidic bubble generator from the premixed gases.

It has been known for a long time that bubbles in water carry a negative charge [15–18]. A similar effect was observed for oil drops in water [19,20]. The experiment showed that ζ-potential of the bubbles (drops) changes with pH from zero at pH = 2–4 up to -120 mV at pH ≈ 10. The surface density of charges measured for oil drops [20] corresponds roughly $n_s = (3-4) \times 10^{13}\ \text{cm}^{-2}$ at neutral pH. For bubbles in water, the charge density is expected to be in the same range, because the pH dependence of the ζ-potential is similar to that for the drops [21].

Significant ζ-potential of the bubbles and drops is typically associated with the adsorption of hydroxyl ions at the interface. However, not all authors support this point of view. For example, it was proposed in [22] that the charge transfer is related to the anisotropy of water–water hydrogen bonding at the interface. Different points of view on the origin of the charges on the interface are reviewed in [21,22] (see original references therein), but the experimental fact that the negative charges exist on the interface is not disputed.

2. Model

We assume that the charges on the bubble walls can play the role of special sites for dissociation of H_2 and possibly O_2 molecules. Although there is no direct experimental evidence for this specific dissociation, the generation of OH free radicals was observed in collapsing microbubbles filled with air, oxygen, or ozone in the absence of external dynamic stimuli [23,24]. The microbubbles with a size smaller than 50 μm decrease in size and collapse softly under water after several minutes. Although pressure in the shrinking bubble increases, temperature does not change significantly because the process proceeds slowly in comparison with acoustically driven bubbles [25,26]. The pressure increase alone is not sufficient to produce radicals, and it was proposed [23] that the charges on the bubble

surface play a role. We believe that surface-assisted reactions have to be involved and the surface charges provides sites for these reactions.

A molecule impinging on a charged site acquires the electrostatic energy $\mathcal{E}_{el} \sim (\alpha_0/4\pi\varepsilon_0)(q/h^2)^2$, where α_0 is the static polarizability of the molecule (for hydrogen $\alpha_0 \approx 0.79$ Å^3), ε_0 is the vacuum permittivity, q is the electric charge of the site, and h is the distance between the site and the molecule. The equilibrium distance due to the van der Waals attraction and the short-range repulsion is about $h = 3$ Å. Using the maximal charge on the site to be the charge of an electron, $q = e$, one finds $\mathcal{E}_{el} \approx 0.14$ eV, which is much smaller than the dissociation energy (4.5 eV for H$_2$). Therefore, direct interaction of the induced dipole with the charged site can play only a marginal role.

In spite of a large dissociation energy, plasmon-induced dissociation of H$_2$ was reported on gold nanoparticles [27,28]. The mechanism includes transition of a hot electron on an antibonding state of an approaching molecule with the following dissociation of H$_2^-$ ion. In our case, if the charged site is OH$^-$, the energy of electron with respect to vacuum is -9.2 eV [29]. It is considerably deeper than the antibonding level in a free hydrogen molecule -3.7 eV [30]. Nevertheless, the electron transfer is possible because the external potential ϕ is applied to the system. The electrochemical potential of OH$^-$ ion is then $\bar{\mu} = \mu + q\phi$, where $\mu = -9.2$ eV is the chemical potential of the ions without the field and q the charge of the ions. On the other hand, the hydrogen molecule is neutral and interacts with the field only via the induced dipole moment. The external potential sweeps from $-\phi_0$ to $+\phi_0$ with a frequency $f \sim 100$ kHz [9]. For sufficiently large amplitude ϕ_0 there is always a moment of time when the electron energy in the ion is equal to the energy of the antibonding level of H$_2$ molecule. Combustion in nanobubbles is observed at a rather high potential $\phi_0 \gtrsim 5$ V [13].

We assume that the radicals are formed in the gas phase as is observed for shrinking microbubbles [23,24]. The process—which we call the "surface assisted dissociation"—differs from the catalytic process, where the products of the dissociation are adsorbed on the surface. The difference can be related to two factors: the gas–liquid interface has no fixed positions for molecules as there are for the gas-solid interface, and the surface charges will push the transitional state out of the wall.

Many details of the proposed mechanism are not clear yet. For example, energy levels of hydrogen can change when a molecule approaches the charged site so as the energy of the solvated OH$^-$ ion at the bubble surface can differ from -9.2 eV. Moreover, it is even debated that the charged sites are related to OH$^-$ ions. Because of the uncertainties, we approach the problem from a different side. It is simply assumed that there are non-zero probabilities for the dissociation of H$_2$ and O$_2$ molecules on the charged sites. Using these probabilities as parameters, we solve the chemical kinetic equations inside of a nanobubble to see if the reaction can be ignited spontaneously at room temperature, and what the main products of the reaction are.

The combustion of hydrogen–oxygen mixture is a well-investigated process [1–4] that is more complex than the one-step overall reaction $2H_2 + O_2 \rightarrow 2H_2O$. The process is controlled by chain branching reactions in the volume competing with the volume and surface termination reactions. The combustion can be ignited spontaneously (see [31,32] on autoignition limits) at moderate temperature ($T > 700$ K), but no combustion is possible at lower temperatures. All species taking part in the reaction include: three molecules H$_2$, O$_2$, and H$_2$O; four short-lived radicals H, O, OH, and HO$_2$, plus one long-lived radical H$_2$O$_2$. Since in this work we consider the processes on nano- and microsecond scales, the latter can be considered as a stable molecule.

If the combustion happens in the nanobubble, the gas temperature during the process can be considered as a constant equal to the temperature of the surrounding liquid. This is because the thermalization time is quite short. It is limited by the heat diffusion in the gas phase; the time needed to reach homogeneous temperature in the bubble is estimated as $\tau_h = (r^2/\pi^2\chi_0) \cdot (P/P_0) \sim 10^{-10}$ s, where $r \sim 50$ nm is the bubble radius and $\chi_0 \approx 0.9 \times 10^{-4}$ m^2/s is the heat diffusion coefficient in the stoichiometric gas mixture at room temperature and normal pressure P_0, and $P = P_0 + 2\gamma/r$ is the pressure in the bubble that includes the Laplace pressure ($\gamma \approx 0.072$ J/m^2 is the surface

tension of the electrolyte). Thus, the heat diffusion is faster than most of the elementary steps of the combustion reaction.

Because of low temperature, the main chain branching reactions $H + O_2 \rightarrow O + OH$ and $O + H_2 \rightarrow H + OH$ are strongly suppressed, and cannot drive the process. Instead, the H and O radicals can be generated at the bubble surface by the dissociation reactions at the charged centers $H_2^s \rightarrow H + H$ and $O_2^s \rightarrow O + O$. These reactions becomes increasingly important for nanobubbles due to large surface-to-volume ratio $S/V = 3/r$. Although we do not yet understand the dissociation mechanism, the surface reaction seems to be the only way to explain combustion in a small volume at room temperature.

The reaction constant for the surface processes can be presented in the following way [1]:

$$K_i^\pm = \frac{\varepsilon_i^\pm}{4} \bar{v}_i \frac{S}{V} \tag{1}$$

where $\bar{v}_i$ is the average thermal velocity of the *i*-th species. The sign "+" corresponds to the surface dissociation reaction, and "−" is related to the surface termination reactions. The parameter $\varepsilon_i^\pm$ can be considered as the probability of the surface reactions. For the radical termination on glass walls, the typical values are in the range $\varepsilon_i^- = 10^{-5} - 10^{-2}$ [1,2]. For the dissociation reactions, ε_i^+ can be presented in the form $\varepsilon_i^+ = \sigma_i n_s$, where σ_i is the dissociation cross-section for hydrogen or oxygen molecules, and n_s is the concentration of the centers for dissociation on the bubble surface. If we relate the centers to the surface charges, this concentration is estimated as $n_s \sim 10^{13} \, \text{cm}^{-2}$. For the cross-section $\sigma \sim 1 \, \text{Å}^2$, one finds the dissociation probability $\varepsilon^+ \sim 10^{-3}$.

3. Combustion Kinetics

We solve the equations of chemical kinetics for eight relevant species H, O, OH, HO_2, H_2, O_2, H_2O, and H_2O_2 enumerated as $i = 1, 2, ..., 8$, respectively. It is assumed that the species are distributed homogeneously in the bubble. This is a good approximation for all molecules and radicals, except maybe hydrogen atoms. For H radicals, the diffusion time $r^2/D_H \sim 10^{-10}$ s—where $D_H \sim 10^{-5} \, \text{m}^2/\text{s}$ is the diffusion coefficient—is comparable with the fastest reaction linear in H. This is the reaction $H + O_2 + M \rightarrow HO_2 + M$ that proceeds with the participation of a third body M. For this process, the reaction time is also on the level of 10^{-10} s, and the diffusion of atoms competes with the reaction. The effect becomes important for bubbles larger than 100 nm in diameter. Here we assume that H atoms are distributed homogeneously in the bubble; therefore, our analysis is applicable for rather small bubbles.

Although the bubbles are small, the gas inside of them can be considered as a continuum medium. This is because the pressure inside the bubble increases with the decrease of the bubble size due to the Laplace pressure. For example, the mean free path λ in a bubble with a radius of $r = 50$ nm is estimated as 4 nm, and λ scales as r. For this reason, the Knudsen number $Kn = \lambda/r \approx 0.08$ stays constant for bubbles, where the Laplace pressure dominates.

The total list of the elementary reactions was taken from Reference [33], but the detailed information on the reaction rates was collected from a number of papers [31,34–41]. The kinetic equations are significantly simplified by the absence of temperature variation in the bubble. In this case, all the reaction rates stay constant during the process. Since nanobubbles with a mixture of gases last less than a few microseconds (combustion can proceed much faster), we select only those reactions that happen on a time scale of 1 µs or faster. The list of these reactions together with the reaction constants at $T = 300$ K and $r = 50$ nm is presented in Table 1. Note that the reverse reactions are not included in the list, because they happen on a time scale longer than 1 µs. The first six processes are the termolecular reactions, and the remaining 13 reactions are the bimolecular reactions. The concentration of all species are defined with respect to the initial gas concentration in the bubble:

$$[M_0] = \frac{P}{RT} \approx 1200 \left(\frac{r_0}{r} \right) \, \text{mol} \cdot \text{m}^{-3} \tag{2}$$

where $T = 300\,\text{K}$, $R = 8.314\,\text{J·mol}^{-1}\text{·K}^{-1}$, $r_0 = 50\,\text{nm}$, and it is assumed that the Laplace pressure dominates in the bubble $P \approx 2\gamma/r$. We define the reaction constants as the probability per unit time, which are related to the standardly defined reaction constants as:

$$K^{(2)} = k^{(2)}[M_0], \quad K^{(3)} = k^{(3)}[M_0]^2 \tag{3}$$

Here $k^{(2)}$ and $k^{(3)}$ have dimensions $\text{m}^3\text{·mol}^{-1}\text{·s}^{-1}$ and $\text{m}^6\text{·mol}^{-2}\text{·s}^{-1}$ for bi- and termolecular reactions, respectively.

Table 1. Bulk reactions included in the network and their reaction constants calculated at $T = 300\,\text{K}$ and $r = 50\,\text{nm}$ according to (3). For termolecular reactions 1–6, the constants are given for M = H_2, O_2, and H_2O, respectively.

	Reaction	$K\text{·ns}^{-1}$	Ref.
1	$H + H + M \rightarrow H_2 + M$	3.4, 5.2, 45	[33,34]
2	$O + O + M \rightarrow O_2 + M$	3.1, 3.6, 2.2	[38,42]
3	$H + O + M \rightarrow OH + M$	90, 61, 500	[35,39,43]
4	$H + OH + M \rightarrow H_2O + M$	240, 285, 2100	[33,37]
5	$H + O_2 + M \rightarrow HO_2 + M$	39, 16, 160	[37,38]
6	$OH + OH + M \rightarrow H_2O_2 + M$	18, 18, 18	[37]
7	$H + HO_2 \rightarrow H_2 + O_2$	3.9	[37]
8	$H + HO_2 \rightarrow H_2O + O$	2.0	[37]
9	$H + HO_2 \rightarrow OH + OH$	50	[37]
10	$H + H_2O_2 \rightarrow HO_2 + H_2$	0.004	[37]
11	$H + H_2O_2 \rightarrow H_2O + OH$	0.03	[37]
12	$O + OH \rightarrow H + O_2$	27	[37]
13	$O + HO_2 \rightarrow OH + O_2$	40	[37]
14	$O + H_2O_2 \rightarrow OH + HO_2$	0.001	[37]
15	$OH + H_2 \rightarrow H_2O + H$	0.004	[37]
16	$OH + OH \rightarrow H_2O + O$	0.9	[37]
17	$OH + HO_2 \rightarrow H_2O + O_2$	77	[37]
18	$OH + H_2O_2 \rightarrow H_2O + HO_2$	1.1	[37]
19	$HO_2 + HO_2 \rightarrow H_2O_2 + O_2$	2.4	[37]

A few comments on Table 1 are in place. The rates of the termolecular reactions depend on the concentration of the third component, [M]. Since the concentration of radicals is always small, as the third body M we consider stable molecules H_2, O_2, H_2O, and H_2O_2. In the third-order reactions 1–6, three numbers correspond to H_2, O_2, and H_2O, respectively. Efficiencies for H_2O and H_2O_2 are considered to be equal. Typically, the reaction rate is measured directly only for one or two components M. The rates for unknown components are predicted using a recommended table of relative efficiencies, such as $Ar:H_2:O_2:H_2O:H_2O_2 = 1:2.8:3.3:17:17$ [33]. For reactions 1–4, the data are available for the pressure up to a few bars. We assume that in the bubble (where the pressure is somewhat higher), these reactions keep the third order. The reaction rates in the low and high pressure limits are known for reaction 5. The transition happens at $[M] = 2500 - 5000\,\text{mol·m}^{-3}$, depending on M. This is higher than the gas concentration in nanobubbles, and the reaction is of the third order. On the contrary, for reaction 6, the transition happens at $[M] \approx 10\,\text{mol·m}^{-3}$, which is much smaller than the concentration in the bubble. Therefore, reaction 6 is effectively of the second order, resulting in equal efficiencies for all M.

Introducing the dimensionless concentrations y_i defined with respect to $[M_0]$ and using 1 ns as the unit of time, we can write the system of eight ordinary differential equations. This system has the following structure:

$$\frac{dy_i}{dt} = R_i^{(3)}(\mathbf{y}) + R_i^{(2)}(\mathbf{y}) + R_i^{(1)}(\mathbf{y}) \tag{4}$$

where $\mathbf{y}$ is a vector with the components y_i, $R_i^{(1,2,3)}(\mathbf{y})$ are the reaction rates for *i*-th species of the first, second, and third order in the concentration. The term $R_i^{(3)}(\mathbf{y})$ includes the first six reactions in Table 1, while the term $R_i^{(2)}(\mathbf{y})$ includes the rest of the reactions in the table. The linear term $R_i^{(1)}(\mathbf{y})$ includes only the surface reactions. For example, for hydrogen atoms this last term can be presented in the form:

$$R_1^{(1)}(\mathbf{y}) = -K_1^- y_1 + 2K_1^+ y_5 \qquad (5)$$

which corresponds to the termination of one H atom at the surface with the probability per unit time K_1^- and creation at the surface of two H atoms from a hydrogen molecule with the probability K_1^+. We introduce nonzero creation terms $K_{1,2}^+$ only for H and O, and the termination terms K_i^- can be nonzero only for radicals H, O, OH, and HO_2 ($i = 1, 2, 3, 4$). Termination of radicals on the surface is considered as permanent, meaning that the radicals sticking to the surface interact within the liquid phase. In this sense, the number of atoms of each kind in the gas phase is not conserved, but it can be considered as a quasi-constant on a time scale of 1 μs.

4. Results

The kinetic Equations (4) were solved numerically with the initial conditions that only hydrogen and oxygen molecules are present in the moment $t = 0$. For the stoichiometric mixture of gases in the initial state, one has $y_5(0) = 2/3$ and $y_6(0) = 1/3$. Suppose that only hydrogen atoms can be produced on the bubble surface and termination of the radicals on the surface can be neglected. A solution that corresponds to the probability of hydrogen dissociation on the surface $\varepsilon_1^+ = 0.003$ is shown in Figure 1. It reaches a quasi-steady-state in 20 ns, and the concentrations vary only on a time scale of ~ 1 μs. In contrast with the standard combustion, the final state contains not only water, but also H_2O_2. The presence of H_2O_2 is a characteristic feature of the surface-assisted combustion. Hydrogen peroxide appears mainly due to reaction 19. If we put the corresponding reaction rate to be zero, the concentration of H_2O_2 is reduced from 0.073 to 0.004. Due to the extra oxygen atom in hydrogen peroxide, not all molecular hydrogen is consumed. A stationary concentration of hydrogen atoms in the final state is due to the absence of the surface termination. Note that the dimensionless termination rate $\varepsilon_i^- \sim 0.001$ gives a much smaller effect than the creation rate $\varepsilon_i^+ \sim 0.001$ because the termination is proportional to a small concentration of radicals. Of course, the concentration of hydrogen atoms cannot stay constant for a long time. It is reduced on a microsecond time scale due to reactions 10 and 11. On the same time scale of 1 μs, the surface termination of H atoms becomes important. All this results in the reduction of H radicals. At $t = 30$ ns, the concentrations of the radicals and molecules are the following: $([H], [O], [OH], [HO_2])/[M_0] = [0.0166, 0, 0, 0]$ and $([H_2], [O_2], [H_2O_2], [H_2O])/[M_0] = [0.0659, 0, 0.0741, 0.5183]$. It is easy to check that the initial relative number of hydrogen atoms equal to 4/3 coincides with that in the finale state and is similar for oxygen atoms.

The generation of hydrogen atoms on the surface is of principal importance. The reaction is not ignited if only oxygen atoms are generated on the surface. At a fixed ε_1^+, the concentration of H_2O_2 slightly decreases relative to water when ε_2^+ increases. The time $\tau_{0.9}$ to reach a steady state strongly depends on ε_1^+, as shown in Figure 2a. We define $\tau_{0.9}$ as the time when water concentration reaches 90% of its stationary value. It is well approximated by the function $\tau_{0.9} \approx 0.13 \times (\varepsilon_1^+)^{-0.834}$ ns. Figure 2b shows how water concentration in the final state depends on ε_1^+ (red curve), and shows the relative concentration of H_2O_2 with respect to H_2O (blue curve) at steady state. For very small ε_1^+, the concentration of hydrogen peroxide becomes comparable to that of water.
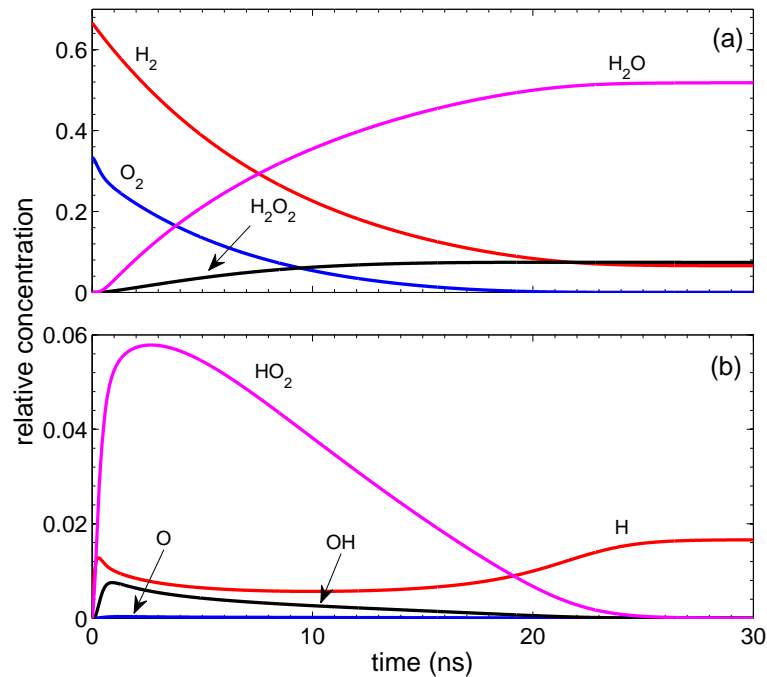
Figure 1. (**a**) Relative concentration of stable molecules as functions of time; (**b**) Concentration of radicals at different moments of time. The solution is presented for $\varepsilon_1^+ = 0.003$, $\varepsilon_2^+ = 0$, and $\varepsilon_i^- = 0$ ($i = 1, 2, 3, 4$).
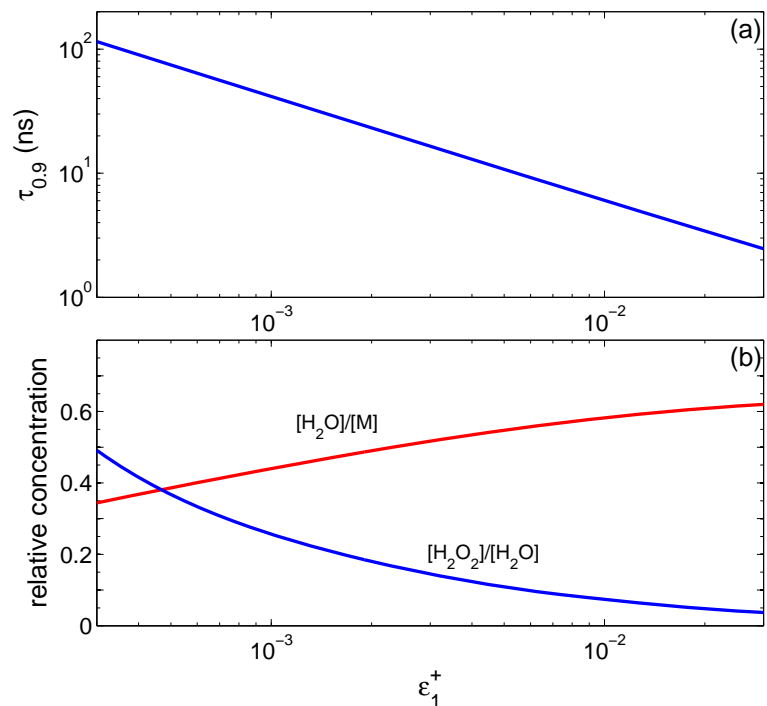
Figure 2. (**a**) Time needed to reach a steady state $\tau_{0.9}$ as a function of the probability of hydrogen dissociation on the surface ε_1^+; (**b**) Water concentration in the steady state (red) and the relative concentration of hydrogen peroxide (blue) as functions of ε_1^+.

Figure 3a shows the dependence of $\tau_{0.9}$ on the initial concentration of oxygen $y_6(0) = ([O_2]/[M_0])_{t=0}$ at the condition that total concentration at $t = 0$ is fixed: $y_5(0) + y_6(0) = 1$. This time has a maximum close to the stoichiometric ratio. Dependence of the peroxide/water ratio in the final

state on the initial concentration of oxygen is shown in Figure 3b. The relative contribution of H_2O_2 increases with the increase of the oxygen fraction in the initial state. The peroxide/water ratio also increases with the decrease of the bubble size r: at $r = 75$ nm it is 0.047, and at $r = 25$ nm it is as large as 0.14.
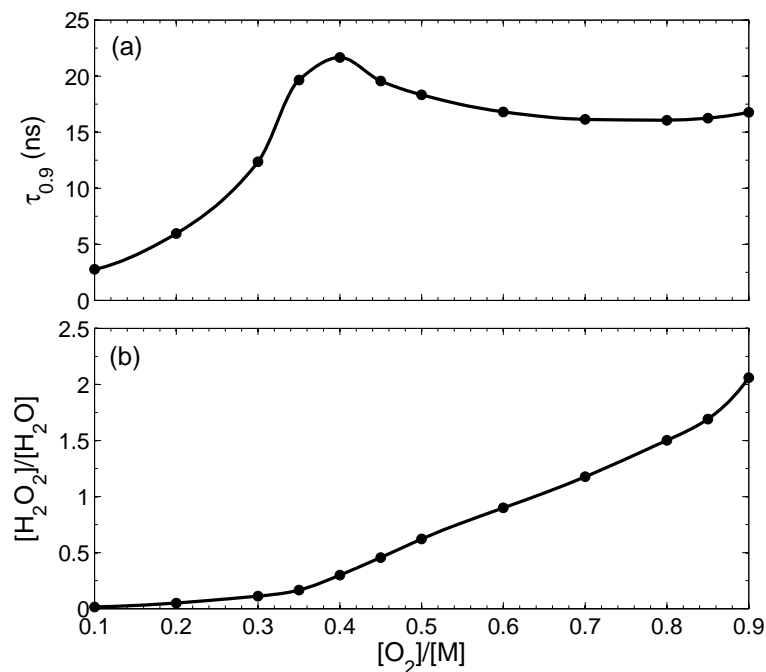
Figure 3. Dependence on the initial concentration of oxygen at a fixed value of the total concentration $[H_2] + [O_2] = [M_0]$. Dots present the points of actual calculation, but smooth curves are drawn by cubic interpolation. (**a**) Time needed to reach the steady state; (**b**) Relative concentration of hydrogen peroxide with respect to water.

Uncertainties in the rates of termolecular reactions do not change the combustion process significantly. For reactions 1–3, we do not know where the transition between high and low pressure limits is. However, if we exclude reactions 2 and 3, the concentrations for all species practically coincide with that presented in Figure 1. Reaction 1 influences the concentrations of H and H_2, but has only a weak effect on all the other components. Qualitatively, the time dependence and the magnitude for all components does not change if we switch off all the termolecular reactions, excepting reaction 5. In absence of reaction 5, the mixture of gases is not ignited.

5. Conclusions

We proposed an explanation of the combustion reaction in nanobubbles, which happens spontaneously at room temperature and cannot be explained in the standard combustion theory. The key step of the mechanism is the dissociation of hydrogen molecules on the charged centers existing on the gas–liquid interface. We kept the dissociation probability as a free parameter and solved the equations of chemical kinetics. It was demonstrated that the combustion is ignited if hydrogen atoms are produced on the bubble walls. The surface-assisted combustion produces in the final state not only water but also an appreciable amount of hydrogen peroxide. The latter is a specific signature that can be used to check the mechanism experimentally. The time scale for combustion in nanobubbles is about 10 ns.

Author Contributions: All the authors formulated the aim and scope of the paper. Niels Tas formulated the idea of the charged centers; Vitaly Svetovoy proposed the chemical kinetics equations with the surface terms; Alexander Prokaznikov developed the model and did calculations; Vitaly Svetovoy wrote the paper; and the writing was reviewed by Niels Tas.

Conflicts of Interest: The authors declare no conflict of interest.

References

1.　Semenov, N.N. *Some Problems in Chemical Kinetics and Reactivity*; Princeton University: Princeton, NJ, USA, 1959; Volume 2.

2.　Lewis, B.; von Elbe, G. *Combustion, Flames and Explosions of Gases*; Academic Press: New York, NY, USA, 1987.

3.　Law, C.K. *Combustion Physics*; Cambridge University: Cambridge, UK, 2006.

4.　Glassman, I.; Yetter, R.A. *Combustion*, 4 ed.; Elsevier: New York, NY, USA, 2008.

5.　Veser, G. Experimental and theoretical investigation of H_2 oxidation in a high-temperature catalytic microreactor. *Chem. Eng. Sci.* **2001**, *56*, 1265–1273.

6.　Fernandez-Pello, A.C. Micropower generation using combustion: Issues and approaches. *Proc. Combust. Inst.* **2002**, *29*, 883–899.

7.　Maruta, K. Micro and mesoscale combustion. *Proc. Combust. Inst.* **2011**, *33*, 125–150.

8.　Chou, S.; Yang, W.; Chua, K.; Li, J.; Zhang, K. Development of micro power generators—A review. *Appl. Energy* **2011**, *88*, 1–16.

9.　Svetovoy, V.B.; Sanders, R.G.P.; Lammerink, T.S.J.; Elwenspoek, M.C. Combustion of hydrogen-oxygen mixture in electrochemically generated nanobubbles. *Phys. Rev. E* **2011**, *84*, doi:10.1103/PhysRevE.84.035302.

10.　Svetovoy, V.B.; Sanders, R.G.P.; Ma, K.; Elwenspoek, M.C. New type of microengine using internal combustion of hydrogen and oxygen. *Sci. Rep.* **2014**, *4*, doi:10.1038/srep04296.

11.　Postnikov, A.V.; Uvarov, I.V.; Prokaznikov, A.V.; Svetovoy, V.B. Observation of spontaneous combustion of hydrogen and oxygen in microbubbles. *Appl. Phys. Lett.* **2016**, *108*, doi:10.1063/1.4944780.

12.　Postnikov, A.V.; Uvarov, I.V.; Lokhanin, M.V.; Svetovoy, V.B. Highly energetic phenomena in water electrolysis. *Sci. Rep.* **2016**, *6*, doi:10.1038/srep39381.

13.　Svetovoy, V.; Postnikov, A.; Uvarov, I.; Sanders, R.; Krijnen, G. Overcoming the fundamental limit: Combustion of a hydrogen-oxygen mixture in micro- and nano-bubbles. *Energies* **2016**, *9*, doi:10.3390/en9020094.

14.　Jain, S.; Mahmood, A.; Qiao, L. Quantifying heat produced during spontaneous combustion of H_2/O_2 nanobubbles. In Proceedings of the 2016 IEEE Sensors, Orlando, FL, USA, 30 October–3 November 2016.

15.　Li, C.; Somasundaran, P. Reversal of bubble charge in multivalent inorganic salt solutions—Effect of magnesium. *J. Colloid Interface Sci.* **1991**, *146*, 215–218.

16.　Graciaa, A.; Morel, G.; Saulner, P.; Lachaise, J.; Schechter, R. The ζ-potential of gas bubbles. *J. Colloid Interface Sci.* **1995**, *172*, 131–136.

17.　Takahashi, M. ζ potential of microbubbles in aqueous solutions: Electrical properties of the gas water interface. *J. Phys. Chem. B* **2005**, *109*, 21858–21864.

18.　Creux, P.; Lachaise, J.; Graciaa, A.; Beattie, J.K. Specific cation effects at the hydroxide-charged air/water interface. *J. Phys. Chem. C* **2007**, *111*, 3753–3755.

19.　Marinova, K.G.; Alargova, R.G.; Denkov, N.D.; Velev, O.D.; Petsev, D.N.; Ivanov, I.B.; Borwankar, R.P. Charging of oil-water interfaces due to spontaneous adsorption of hydroxyl ions. *Langmuir* **1996**, *12*, 2045–2051.

20.　Beattie, J.K.; Djerdjev, A.M. The pristine oil/water interface: Surfactant-free hydroxide-charged emulsions. *Angew. Chem. Int. Ed.* **2004**, *43*, 3568–3571.

21.　Beattie, J.K.; Djerdjev, A.M.; Warr, G.G. The surface of neat water is basic. *Faraday Discuss.* **2009**, *141*, 31–39.

22.　Vácha, R.; Marsalek, O.; Willard, A.P.; Bonthuis, D.J.; Netz, R.R.; Jungwirth, P. Charge transfer between water molecules as the possible origin of the observed charging at the surface of pure water. *J. Phys. Chem. Lett.* **2012**, *3*, 107–111.

23.　Takahashi, M.; Chiba, K.; Li, P. Free-radical generation from collapsing microbubbles in the absence of a dynamic stimulus. *J. Phys. Chem. B* **2007**, *111*, 1343–1347.

24.　Li, P.; Takahashi, M.; Chiba, K. Enhanced free-radical generation by shrinking microbubbles using a copper catalyst. *Chemosphere* **2009**, *77*, 1157–1160.

25.　Brennen, C.E. *Cavitation and Bubble Dynamics*; Oxford University Press: Oxford, UK, 1995.

26. Didenko, Y.T.; Suslick, K.S. The energy efficiency of formation of photons, radicals and ions during single-bubble cavitation. *Nature* **2002**, *418*, 394–397.

27. Mukherjee, S.; Libisch, F.; Large, N.; Neumann, O.; Brown, L.V.; Cheng, J.; Lassiter, J.B.; Carter, E.A.; Nordlander, P.; Halas, N.J. Hot electrons do the impossible: Plasmon-induced dissociation of H_2 on Au. *Nano Lett.* **2013**, *13*, 240–247.

28. Libisch, F.; Cheng, J.; Carter, E. Electron-transfer-induced dissociation of H_2 on gold nanoparticles: Excited-state potential energy surfaces via embedded correlated wavefunction theory. *Z. Phys. Chem.* **2013**, *227*, 1455–1466.

29. Winter, B.; Faubel, M.; Hertel, I.V.; Pettenkofer, C.; Bradforth, S.E.; Jagoda-Cwiklik, B.; Cwiklik, L.; Jungwirth, P. Electron binding energies of hydrated H_3O^+ and OH^-: Photoelectron spectroscopy of aqueous acid and base solutions combined with electronic structure calculations. *J. Am. Chem. Soc.* **2006**, *128*, 3864–3865.

30. Schulz, G.J.; Asundi, R.K. Formation of H^- by electron impact on H_2 at low energy. *Phys. Rev. Lett.* **1965**, *15*, 946–949.

31. Azatyan, A.A.; Andrianova, Z.S.; Ivanova, A.N. Role of the HO_2 radical in hydrogen oxidation at the third self-ignition limit. *Kinet. Catal.* **2010**, *51*, 337–347.

32. Wang, X.; Law, C.K. An analysis of the explosion limits of hydrogen-oxygen mixtures. *J. Chem. Phys.* **2013**, *138*, doi:10.1063/1.4798459.

33. Gerasimov, G.Y.; Shatalov, O.P. Kinetic mechanism of combustion of hydrogen–oxygen mixtures. *J. Eng. Phys. Thermophys.* **2013**, *86*, 987–995.

34. Cohen, N.; Westberg, K.R. Chemical kinetic data sheets for high-temperature chemical reactions. *J. Phys. Chem. Ref. Data* **1983**, *12*, 531–590.

35. Tsang, W.; Hampson, R.F. Chemical kinetic data base for combustion chemistry. Part I. Methane and related compounds. *J. Phys. Chem. Ref. Data* **1986**, *15*, 1087–1279.

36. Ó Conaire, M.; Curran, H.J.; Simmie, J.M.; Pitz, W.J.; Westbrook, C.K. A comprehensive modeling study of hydrogen oxidation. *Int. J. Chem. Kinet.* **2004**, *36*, 603–622.

37. Baulch, D.L.; Bowman, C.T.; Cobos, C.J.; Cox, R.A.; Just, T.; Kerr, J.A.; Pilling, M.J.; Stocker, D.; Troe, J.; Tsang, W.; et al. Evaluated kinetic data for combustion modeling: Supplement II. *J. Phys. Chem. Ref. Data* **2005**, *34*, 757–1397.

38. Konnov, A.A. Remaining uncertainties in the kinetic mechanism of hydrogen combustion. *Comb. Flame* **2008**, *152*, 507–528.

39. Ibragimova, L.B.; Smekhov, G.D.; Shatalov, O.P. Comparative Analysis of Kinetic Mechanisms of Hydrogen- Oxygen Mixtures. Available online: www.chemphys.edu.ru/pdf/2009-06-29-001.pdf (accessed on 29 June 2009).

40. Hong, Z.; Davidson, D.F.; Hanson, R.K. An improved H_2/O_2 mechanism based on recent shock tube/laser absorption measurements. *Comb. Flame* **2011**, *158*, 633–644.

41. Burke, M.P.; Chaos, M.; Ju, Y.; Dryer, F.L.; Klippenstein, S.J. Comprehensive H_2/O_2 kinetic model for high-pressure combustion. *Int. J. Chem. Kinet.* **2012**, *44*, 444–474.

42. Warnatz, J. Rate coefficients in the C/H/O system. In *Combustion Chemistry*; Gardiner, W.C., Ed.; Springer-Verlag: New York, NY, USA, 1984.

43. Javoy, S.; Naudet, V.; Abid, S.; Paillard, C. Elementary reaction kinetics studies of interest in H_2 supersonic combustion chemistry. *Exp. Therm. Fluid Sci.* **2003**, *27*, 371–377.